Magazine of Civil Engineering

ISSN 2712-8172

journal homepage: http://engstroy.spbstu.ru/

Research article

UDC 624.03

DOI: 10.34910/MCE.117.3

Numerical analysis of the buried fiber concrete slabs dynamics under blast loads

A.V. Alekseytsev ✉ , ***S.A. Sazonova***

Moscow State University of Civil Engineering (National Research University), Moscow, Russia

✉ *aalexw@mail.ru*

Keywords: FRC, blast load, mechanical safety, numerical analysis, deformable supports, implicit dynamic simulation, strength, progressive collapse, damping

Abstract. The approach to numerical modeling of fiber reinforced concrete slab (FRCS) under blast load is considered. The slab is used for coverings of buried protective structures. The stress-strain state of this structure is investigated in the dynamic setting. The loads in this case change in time in terms of both intensity and area. The calculation makes provision for the consideration of rigid and deformable structure of support units. The damping properties of the structure are evaluated for its resistance to progressive collapse. Concrete dilatation and softening are factored in the numerical simulation. The bond between the fiber concrete and the reinforcement was modeled by introducing interpolation elements that simulate the absence of deformation in the area of their contact. The interaction of FRCS with the deformed support was modeled using the linear contact. The transition from the elastic-plastic deformation stage to the rigid stage was performed by introducing gap elements. The geometric nonlinearity, as well as the physical nonlinearity for fiber-reinforced concrete and reinforcement, was taken into account in estimating the ultimate loading. The load absorbed by the structure through the thickness of the ground during detonation explosion of a charge on its surface was considered. To realize numerical integration of the system motion equations, an implicit scheme was used. It is based on a modification of the Newmark step method in which effective matrices of fiber concrete and reinforcement stiffness are constructed at each step considering the loading history of the structure for its deformed state. The possibility of effective regulation of the stress-strain state of FRCS was established, which allows the design of effective and safe structures of this type.

Citation: Alekseytsev, A.V., Sazonova, S.A. Numerical analysis of the buried fiber concrete slabs dynamics under blast loads. Magazine of Civil Engineering. 2023. 117(1). Article no. 11703. DOI: 10.34910/MCE.117.3

1. Introduction

In connection with the need to ensure the mechanical safety of load-bearing structures under special influences, the topic of the article is relevant. External challenges require the design of new structures and reconstruction of existing buried protective structures. At the same time, the impacts from soil, transferred to the structure, most often have the highest intensity for the cover slabs. The results of deformation analysis and design of bearing systems under such impacts show that a significant increase in material intensity of bearing systems is required to ensure mechanical safety [1–5]. In addition, the choice of dynamic calculation methodology is of interest. A number of works [6–8] are aimed at the investigation of the dynamics of building structures with high loading rates. In this case, explicit solvers are most often used, and the criterion for material failure is often equivalent von Mises stresses. Such works are devoted to the resistance to explosive loads for reinforced concrete and steel frames [9–13], plates [14–18], for panels of steel plates with corrugated middle layers [4, 7, 19, 20], etc.

The study of the dynamics of structures with low impact velocities is characteristic when assessing the resistance to progressive collapse of structures at local mechanical damage [21–26], at combined

damage [27]. For such calculations with relatively long transient dynamic process time, implicit integration schemes can be effectively used [28–30].

Reducing the consumption of materials for supporting structures under dynamic loads can be achieved by regulating the values of the spectrum vibrations that can be excited by the dynamic action. Such regulation is possible by changing the configuration or supports stiffnesses, as well as by introducing additional devices [31, 32]. In analytical studies of this issue, there are certain difficulties with implementation for engineering calculations. Therefore, numerical simulation is currently the only way to solve this kind of problems in an approximate manner. The search for rational stiffnesses of supports in the dynamic formulation of calculation problems is very time consuming. The selection of optimum values by manual method seems to be ineffective, so to solve these problems it is preferable to use optimization methods. Among many of these methods, it is reasonable to use both gradient and probabilistic approaches [33–35].

Another equally important task is the modeling of dynamic loads on structures [36–40]. For low-velocity dynamics and for relatively simple structures, a simplified energy approach can be applied, according to which the dynamic force can be calculated as the difference between the doubled value of the static force in the calculation of a damaged structure and the static force for an undamaged structure. However, this approach can be applied when the basic form of oscillations excited by the dynamic action coincides with the deformed pattern from the action of the static load. In a number of cases, in particular, when the load changes in time and in the area of action on the structure, it is impossible to use a static equivalent.

Consideration of the transient dynamics of structures is closely related to the use of the damping model. Often the Rayleigh scheme is used, which allows taking into account the damping of vibrations in the medium (inertial damping) and the damping of vibrations as a result of internal friction in the material (structural damping). In this calculation accuracy depends on the values of coefficients α and β. There are also other models, such as the Kelvin-Voigt, nonlocal in time model [41]. To determine the damping properties of structures, a number of experimental studies have been performed, for example [42], which found that the coefficient β varies within a fairly wide range of 0.01–0.2, depending on the design of nodes and the degree of structural damage. For the case we are considering, no values for the α coefficient are given in the literature. This is due to the fact that the medium in which the vibrations occur includes two phases with significantly different properties. On the top of this medium is represented by the ground, and on the bottom – it is air.

This paper considers an approach to modeling fiber reinforced concrete slab (FRCS) under area-variable dynamic loads. The slab is considered to be buried in dense soil. An explosion at the ground surface is considered as the initial momentum. The symmetric and asymmetric effects of the blast load pulse are considered. The analysis of dynamic displacements of the structure and deformations of materials with changes in the stiffness of the support joints is performed.

2. Methods

2.1. Statement of the problem

Examine an explosion on the surface of the ground, which affects the structure buried in the ground by depth h (Fig. 1 a). In the general case of the detonation type of explosion, there are two phases: discharge and compression. The character of change in the initial pulse during the duration of these phases is shown in Fig. 1 b [43]. The influence of the duration of the discharge phase τ_1 on the load transmitted to the RFCS buried in the ground was not considered. Assume that the explosion energy is transmitted to the ground and then to the structure for a time of τ_2. In this case, the blast wave front D can be transferred to the slab both symmetrically and asymmetrically (Fig. 1 d). The process of oscillations of the mechanical system "structure-soil" under explosive impacts is a complex little-studied problem. However, in [43] the results of numerical simulation of blast wave propagation in the ground with transmission to the structure as a function of the depth $h_1 - h_3$ for dense three-phase soil (Fig. 1 c) are presented. Given this time distribution of pressure, it is assumed that the structure-soil system interacts on the basis of one-sided contact. The contact elements have compressive stiffness $EA >> 0$ and tensile stiffness $EA \approx 0$.

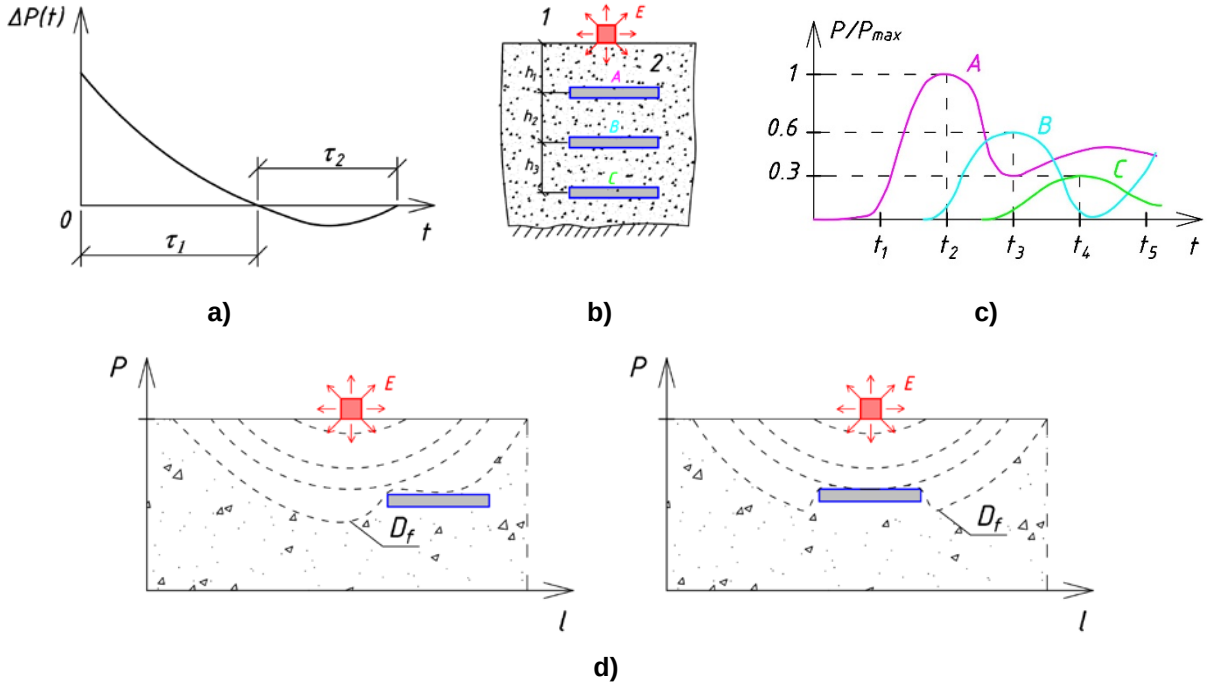

Figure 1. Initial data for modeling the blast load.

2.2. Modeling of blast loads

The initial explosion intensity is characterized by a pulse value (Fig. 1 a), which can be determined on the basis of the experimentally verified Johnes-Wilkins-Lee (JWL) model:

$$P = A\left(1-\frac{\omega}{R_1 V}\right)e^{-R_1 V} + B\left(1-\frac{\omega}{R_2 V}\right)e^{-R_2 V} + \frac{\omega E}{V}, \quad (1)$$

where the values A, B, R_1, R_2, ω, E are constants, which are determined on the basis of the methods of works [44, 45], V is the relative volume of explosive substance, determined by the method JWL. As an example of a reference explosion for TNT, values A = 3.712 Mbar, B = 0.0323 Mbar, R_1 = 4.15, R_2 = 0.95, ω = 0.3, E = 0.07 Mbar are given in [46].

Based on the oscillation graph shown in Fig. 1 c, consider that the pulse impact $\tilde{i}$ can be represented in the form of an equivalent load q_{eq}, acting for time t:

$$\tilde{i} = \mu P \tau_2 / 2 = q_{eq} t, \quad (2)$$

where μ is the coefficient of maximum pulse reduction due to structural burial, t is the action time of the equivalent load q_{eq}.

Considering the duration τ_2 of the compression phase and assuming the magnitude $t \approx 0.2T$, it is possible to represent the load on the structure as a sum:

$$F(t) = q_{st} f_{st}(t) + \sum_{i=1}^{S} q_{i,eq} f_i(t), \quad (3)$$

where q_{st} is the intensity of constant loads, $f_{st}(t)$ is the unit function of change in static load introduced to ensure the stability of the numerical integration procedure, $q_{i,eq}$ is the maximum intensity of dynamic load of i type, S is the number of functions modeling the change in load in time by area and intensity, $f_i(t)$ this is the unit function of change in time of dynamic load. The type of these functions is presented in section 3.1.

2.3. Modeling of FRCS deformations

The problem is solved in a dynamic formulation based on an implicit scheme for numerical integration of the equations:

$$M\,\ddot{\vec{y}} + C\,\dot{\vec{y}} + K_\tau \vec{y} = \vec{F} + \vec{G}\chi, \tag{4}$$

where M is the mass matrix, C is the damping matrix, K_τ is the general tangent stiffness matrix for the finite element system, $\vec{y}$ is the displacement vector, $\dot{\vec{y}}$, $\ddot{\vec{y}}$ are the vectors of first and second derivatives of displacements, $\vec{F}$, $\vec{G}$, is the vectors of nodal forces from external dynamic loads and gravity forces respectively, χ is the Heaviside function equal to one at $t > 0$ else $\chi = 0$.

The matrix C is defined as follows:

$$C = \beta K_\tau;\; K_\tau = K_{bo} + K_{so} + K_{po} + K_{co} + K_{b\sigma} + K_{s\sigma} + K_{p\sigma}, \tag{5}$$

where K_{bo}, K_{so}, K_{po} are, respectively, the deformation matrices for fiber concrete, reinforcement, and supports (when considering non rigid supports), K_{co} is the stiffness matrix of the contact finite elements, $K_{b\sigma}$, $K_{s\sigma}$, $K_{p\sigma}$ are the geometric matrices for fiber concrete, reinforcement, and supports.

Fibre concrete is modeled by hexahedral solid elements, for which the Drucker-Prager material model is implemented, determined by the concrete internal friction angle $\tilde{\varphi}$ and cohesion stress $\tilde{c}$; the presence of fibre in the concrete is modeled by increasing the design tensile strength R_{bt}. A polymeric fiber is considered, for which the design compressive resistance R_b of fiber concrete is taken equal to that of the concrete matrix Consideration of dilatation is performed for the level of relative stresses $\sigma/R_b \geq$ 0.3, with subsequent softening when stresses $\sigma = R_b$ are reached. Rebars are modeled by means of spatial rod elements deforming in accordance with the Prandtl elastoplastic model. The yield criterion is the equivalent Mises stresses, the fracture criterion is the level of deformation exceeding the value 0.025. In the case of modeling of deformable support structures, shell elements deformed elastoplastically without hardening are used.

2.4. Modeling the contact interaction

There are two types of contact interaction in the problem under consideration (Fig. 2 a). The first one simulates a one-sided connection of the structure with the above ground. Simplified, this connection can be modeled by an element of GAP type working only in compression. The first node of the element is connected to the structure, the second node is connected to a point mass from the action of the ground. The ground is considered to be unbound particles as a result of the passage of the blast wave. The second type of contact determines the interaction of FRCS with the supporting structure (Fig. 2 b).

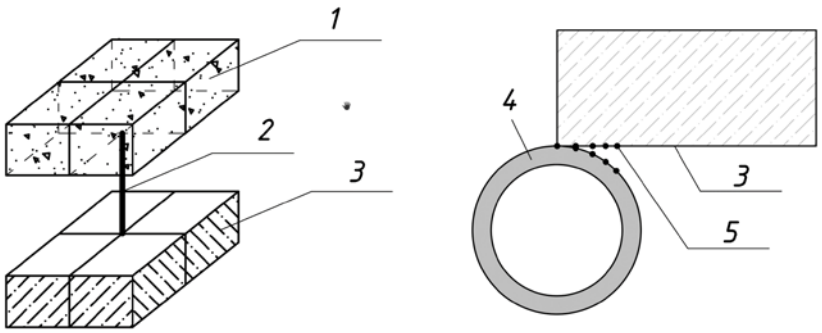

a) **b)**

Figure 2. Contact interaction types: 1 – ground, 2 – GAP element, 3 – FRCS, 4 – damping support, 5 – contact search nodes.

This contact is of the "surface-surface" type and, taking into account the small variations in rotation angles during oscillations in the supports, is accepted as glue. The friction in this contact in the plane of the plate is not taken into account in the case of additional attachment of the support to the plate with anchors. The distance to find the nodes glued in the contact interaction is assumed to be 5 mm. If the elastoplastic

structure of the support has significant deformations, causing its transition to the rigid phase of deformation, GAP-type elements can also be used for this purpose.

3. Results and Discussion

3.1. Input data and model description

Consider the FRCS structure, which is part of the covering of the structure. Lateral loads transferred from the explosion to the structure are not considered. The geometry of the slab is shown in Fig. 3 a, b. The dimensions are taken from the album U 01-01-/80 "Unified prefabricated monolithic structures of buried premises with beam type slabs". The reinforcement scheme was adopted as a typical one. Initially, a 3D-solid model for fiber concrete and a reinforcement cage model in the form of lines were made. This model was imported into the Femap 2021.2 preprocessor where the finite element model was created.

3.1.1. Simulation of loads

Two types of loads were considered in accordance with Fig. 1 d. Modeling of dynamic loading by explosive load transmitted through the ground to the structure was performed as follows. To reproduce the distribution of the load over the area, divide the slab into 5 sections Fig. 4 b.

To describe the symmetrical momentum propagation scenario, and we will use the time functions (Fig. 4 a) for each of the loads $q_1 - q_3$. The load taken by the plate during normal operation is denoted by the variable q_4. It increases for 0.5 sec and remains constant over the entire integration time interval. The residual load intensity in $0.3q$ for each of loads $q_1(t)$, $q_2(t)$, $q_3(t)$ approximates the additional load from the structure-disturbed soil. The distribution of the load in time, taking into account the summation for each moment of time, is shown in Fig. 4 b.

Five different time functions $f_1 - f_5$ are used to describe the asymmetric loading scenario. Their formation is similar to Fig. 4 a, and the summation of the loads for each time moment gives the load distribution shown in Fig. 4 c.

3.1.2. Material Models and Finite Elements

Fibre concrete with non-metallic fiber for FRCS was modeled based on the Drucker-Prager failure criterion described by the following equation:

$$\sqrt{\frac{1}{6}\left[(\sigma_1-\sigma_2)^2+(\sigma_2-\sigma_3)^2+(\sigma_1-\sigma_3)^2\right]} = A+B(\sigma_1+\sigma_2+\sigma_3), \quad (6)$$

where σ_1, σ_2, σ_3 are the principial stresses in the fiber concrete, and $\sigma_1 > \sigma_2 > \sigma_3$.

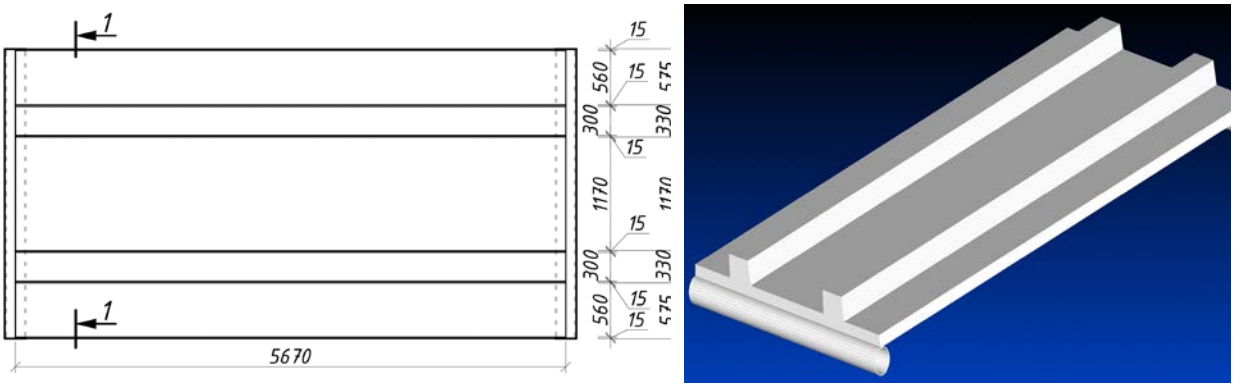

a) d)

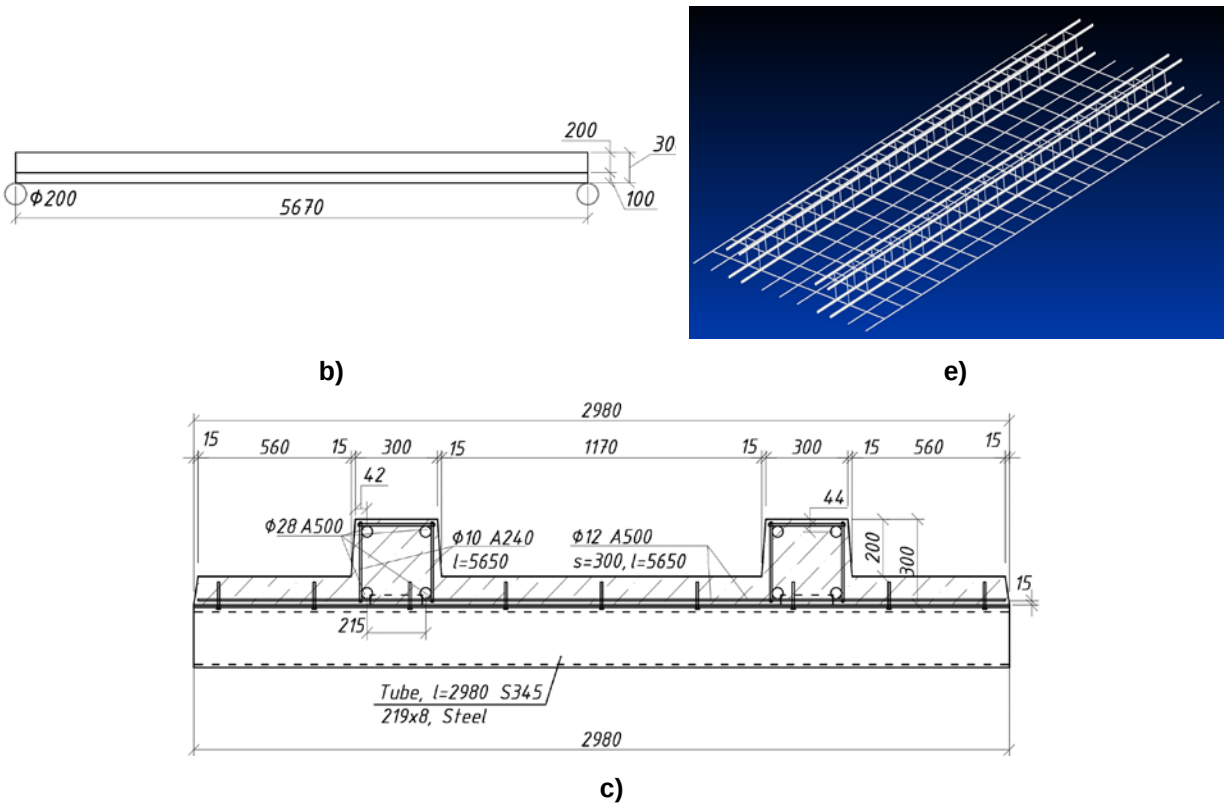

Figure 3. Geometry and model of FRCS.

Where the constants are:

$$A = \frac{2}{\sqrt{3}}\left(\frac{R_b R_{bt}}{R_b + R_{bt}}\right),\ B = \frac{2}{\sqrt{3}}\left(\frac{R_{bt} - R_b}{R_b + R_{bt}}\right), \tag{7}$$

where R_{bt} is the limit design tensile stress in fiber concrete, R_b is the limit design compressive stress. The initial parameters of fiber concrete presented in Table 1 were used.

This criterion (6) was chosen from the considerations of modeling the plastic work of fiber concrete together with the reinforcement in estimating the ultimate loading of the structure. The Drucker-Prager model allows for dilatation under loading as well as softening of the material during the pre-fracture stage. At the same time, there are a number of strength models, such as Mohr-Coulomb, Willam-Warnke, geological CAP model and others, which allow modeling the deformations of concrete and reinforced concrete as a three-dimensional body.

Table 1. Parameters of the fiber concrete deformation model

Compressive strength R_b, MPa	Tensile strength R_{bt}, MPa	Angle of internal friction φ, deg.	Cohesion C, MPa	Angle of dilatation, deg.	Dilatation level σ/R_b
11.5	4.0	35	3.0	25	0.8

A bilinear model with a tangent modulus equal to zero is used to simulate the deformations of the reinforcement and steel pipe. For the reinforcement, equivalent von Mises stresses R_s = 420 MPa are taken as yield stresses. For steel pipes the yield stresses is R_y = 325 MPa.

The fiber concrete was represented by coordinated hexahedral solid elements, which were connected to the rod elements 1 of the rebars (Fig. 5 b). For such connections, interpolation elements 2 were used under the hypothesis of rigid coupling of fiber concrete and reinforcement. In this case, the connection node 3 of the interpolated rigid element 2 with the fiber concrete has a dependence on the linear displacements and angles of rotation from the connection node with the reinforcement. If it is assumed that during deformation the contact determining the bond between the concrete and the reinforcement is pliable, then BEAM or GAP elements can be used as connection elements 2 for which a shear stiffness function is specified.

The partitioning of the solid geometric object for fiber concrete was accepted with the maximum size of the finite elements not more than 0.05 m. The rod elements have a partitioning step of 0.01 m. The finite elements of the plates on the supports have a size of 0.05 m.

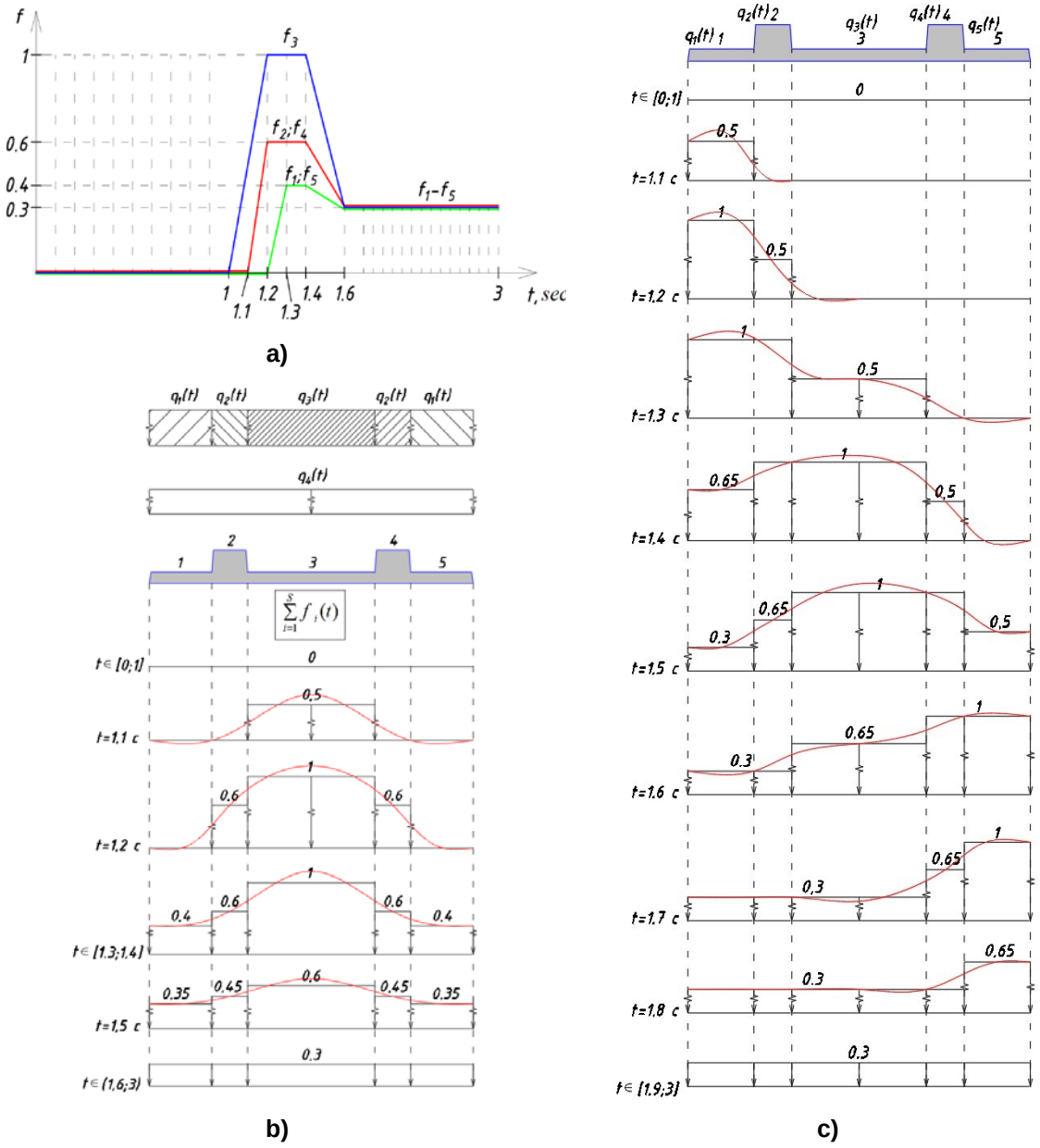

Figure 4. Distribution of dynamic load in time.

The softening function shown in Fig. 5, a is used, which simulates the fracture of fiber concrete when the level of ultimate strain reaches the value 0.0035.

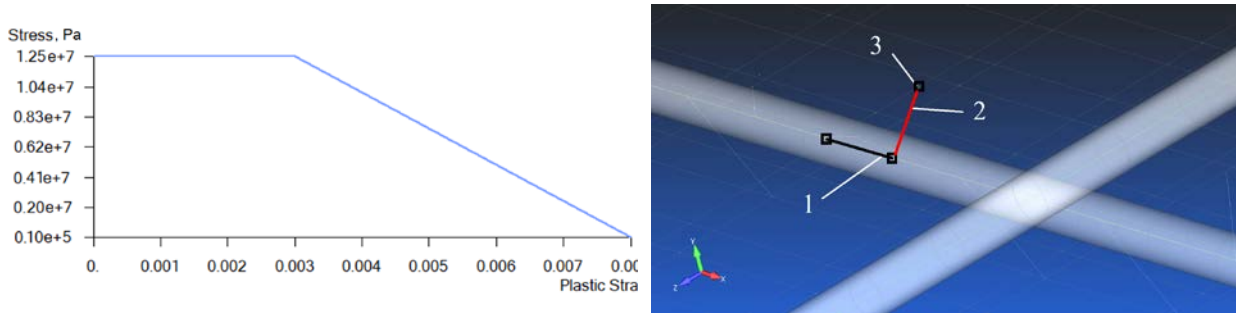

Figure 5. Function of fiber concrete softening and model of its adhesion with reinforcement: 1 – rebar; 2 – interpolation element; 3 – fibercrete element node.

3.1.3. Kinematic constraints

Two cases of support fixtures were considered:

- hinged fixed support at the right edge of FRCS and hinged moving support at the left edge (CS1);
- the same support conditions, but in the zone of pipe contact with the wall of a reinforced concrete buried structure (CS2).

When considering symmetric loading, the supports only support compressive forces. In asymmetric loading, pipe detachment from the FRCS can be observed. In this calculation, this detachment does not occur due to the anchors introduced connecting the FRCS to the pipe and spaced 350 mm apart. For vertical deformations of the pipe, the support assembly is assumed such that there are no restrictions on horizontal deformations. Otherwise, GAP elements can be used to simulate this constraint.

3.2. Model verification. Ultimate static loading

3.2.1. Compression model of fiber concrete prism

To determine the values of cohesion stresses and the angle of internal friction given in Table 1, a numerical calculation up to failure of a standard 30×30×90 mm fiber concrete prism was performed. The Drucker-Prager plasticity model was used. The condition for achieving failure is the value of compressive stresses $\sigma_c = R_b$, and for tensile stresses – $\sigma_t = R_{bt}$. The test results of the prism are shown in Fig. 6, C = 3.0 MPa, φ = 35°.

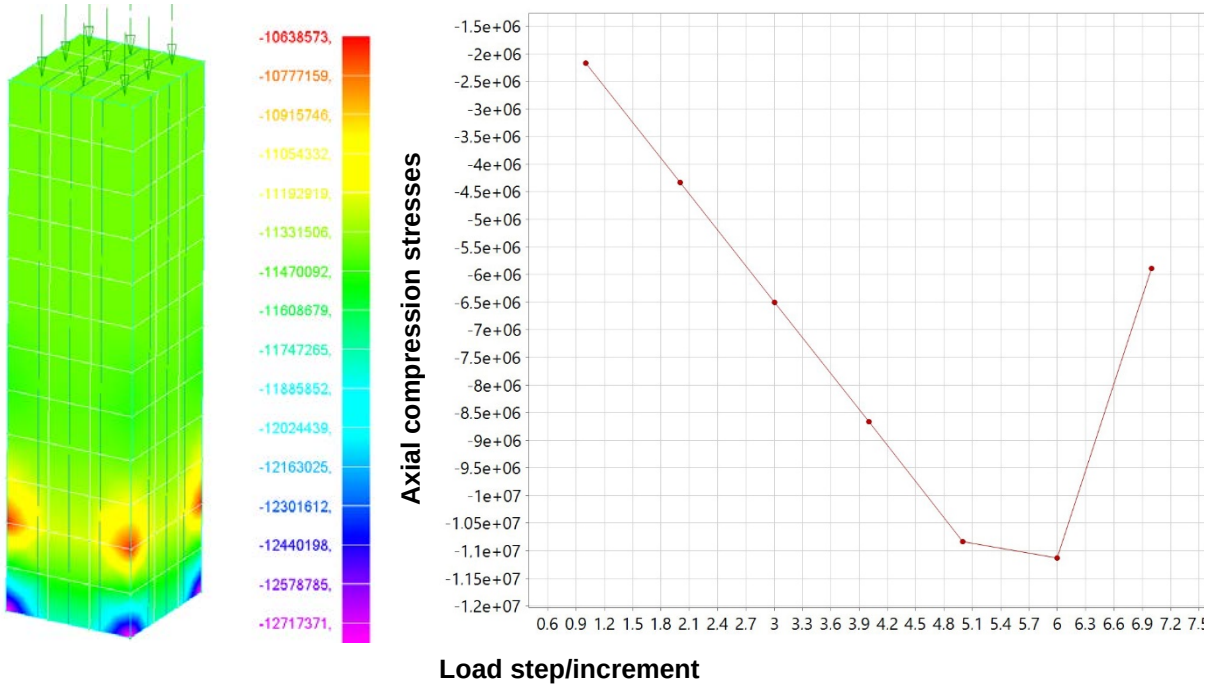

Figure 6. Results of the verification of the computational model.

3.2.2. Static calculation results

The calculation was performed for the action of a load uniformly distributed over the area of the structure. To account for physical nonlinearity, the Newton-Raphson method was used with a force unconstraint equal to 0.001. At each step, 25 iterations were considered. Reaching the limit load level was fixed in the state just before the formation of the mechanism. That is, when the stiffness matrix of the system became ill-conditioned or its determinant was equal to zero. The sequential additional loading assumed 50 steps of 2 kN/m^2 at each step. At 21 steps the calculation was interrupted. As a result, a maximum load of 40 kN/m^2 was determined. The maximum deflection of the slab was 8.5 cm. The distribution of axial longitudinal stresses in the fiber concrete is shown in Fig. 7.

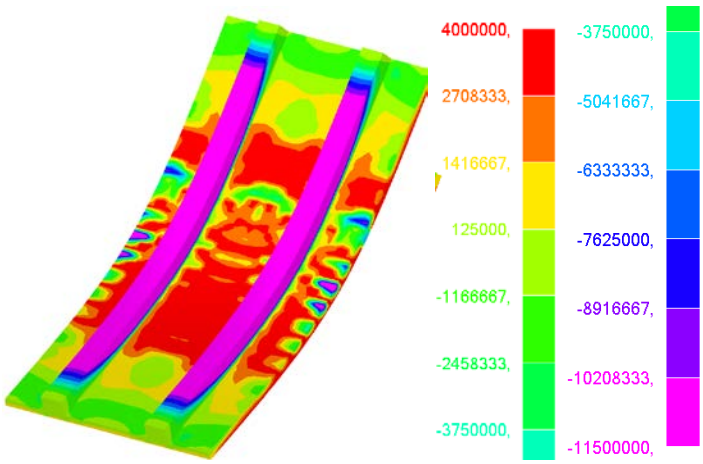

Figure 7. Results of static analysis for FRC, kN/m2.

At the same time through cracks are formed in the slab part and the fiber concrete goes out of operation, transferring the load to the reinforcement mesh and beams. The stresses in the reinforcement reach the yield strength. At the level of load of 20 kN/m^2 the transition of the slab to the limit state starts, which indicates the correctness of the chosen model with its standard operational load of 18 kN/m^2, including its own weight of 3 kN/m^2 and the weight of the overlying 1 m thick soil – 15 kN/m^2 (the value is taken from the album of typical solutions U 01-01-/80 "Unified precast-monolithic structures of underground premises with beam type slabs").

3.3. Dynamic loads

3.3.1. Symmetrical influences

The stress change fields in the fiber concrete in time are shown in Fig. 8. When an explosive load is transmitted through the ground, the entire fiber concrete slab of the FRCS goes out of operation in 0.6 s, and the reinforcement works as a cable structural system. By the time of 2.0 sec the top layer of fiber concrete is destroyed. In this case, as can be seen in the graph (Fig. 9 a) of stresses change in the lower working rebars in time, the stresses in this reinforcement reach the yield strength.

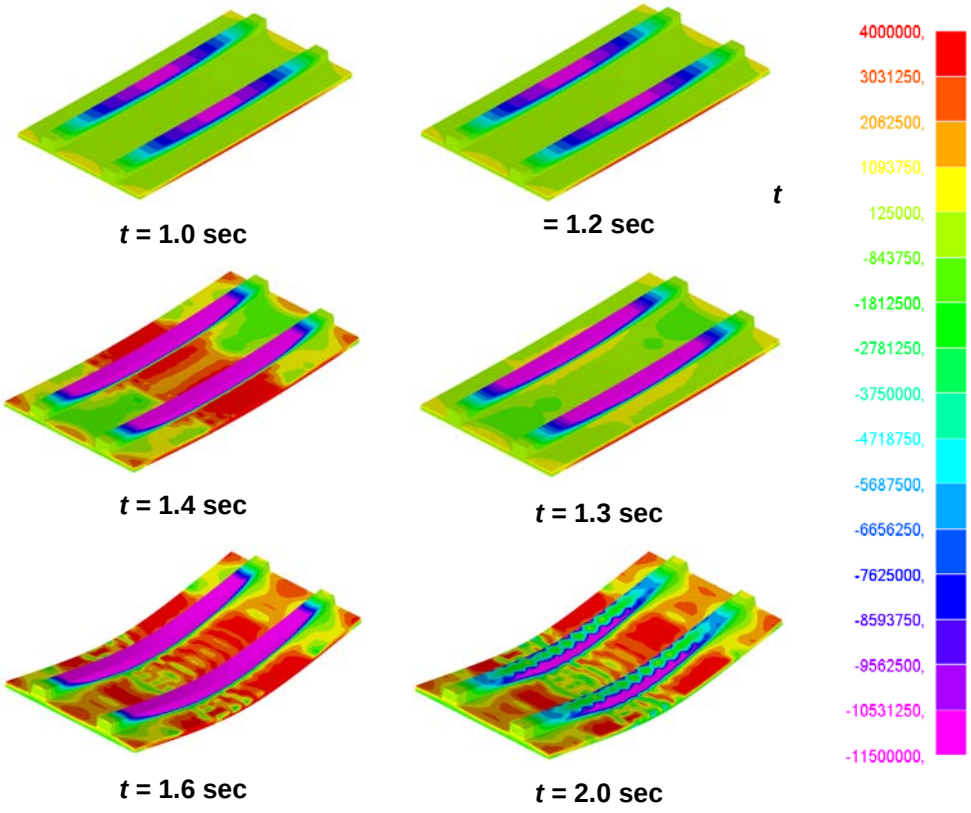

Figure 8. Stress state of fiber concrete under dynamic impact from blast load transmitted through the ground.

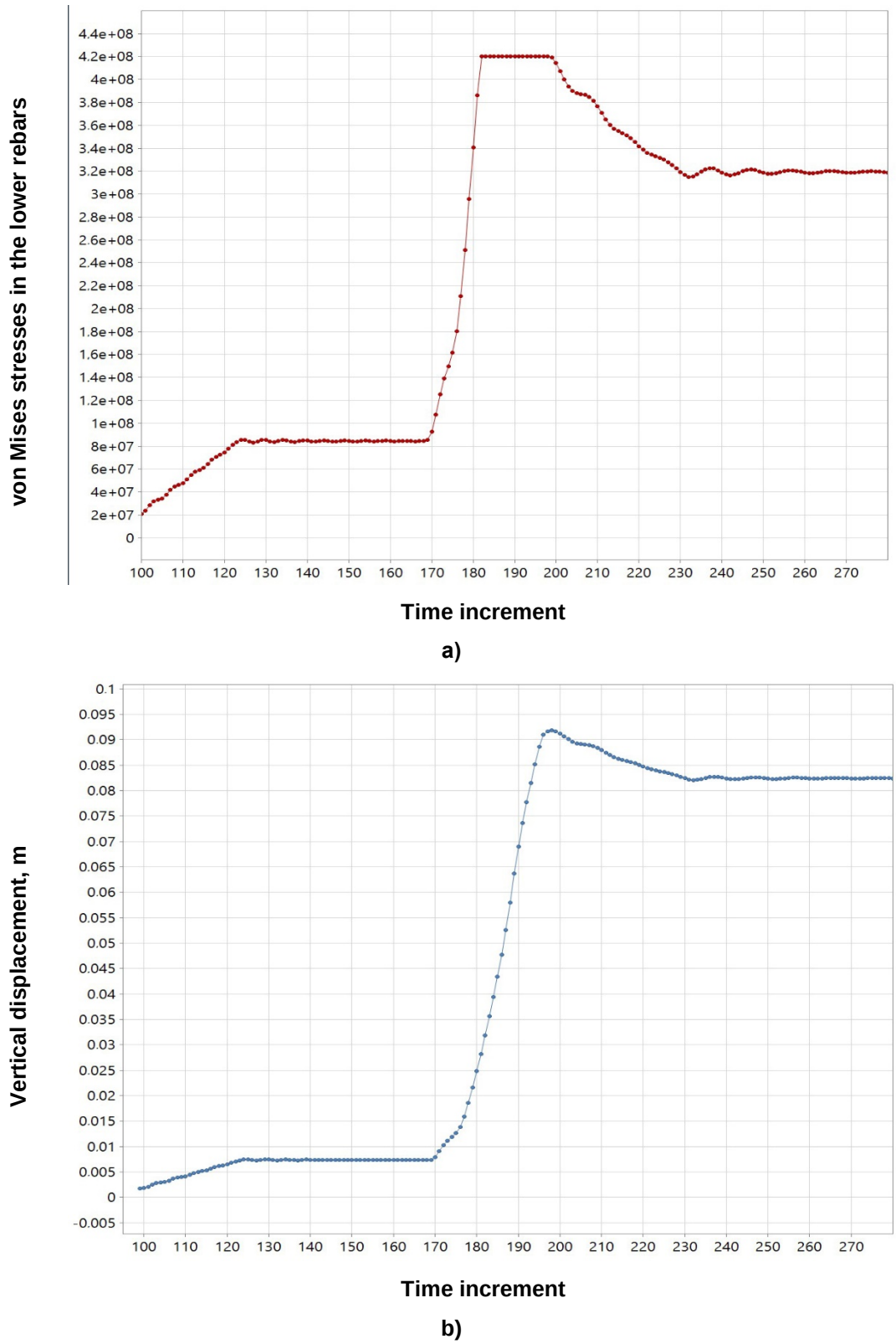

Figure 9. Character of changes in the components of the stress-strain state in time: (a) – displacements; (b) – von Mises stresses in the lower rebars.

The oscillations of the system are damped quite rapidly, the character of this damping is not harmonic due to the significant damping by the fractured soil. The graph of changes in the structure's displacements in time for the characteristic point in the middle of the span is shown in Fig. 9 b. When the anchoring variant (CS1) was used in the system, the system collapsed on the fiber concrete with a load exceeding 25 kPa. The introduction of a deformable tubular support (CS2) did not cause the structure to collapse up to a load of 38 kPa, which has a significant effect in improving the safety of such a structure. At the same time, the tubular support deformed in time as shown in Fig. 10.

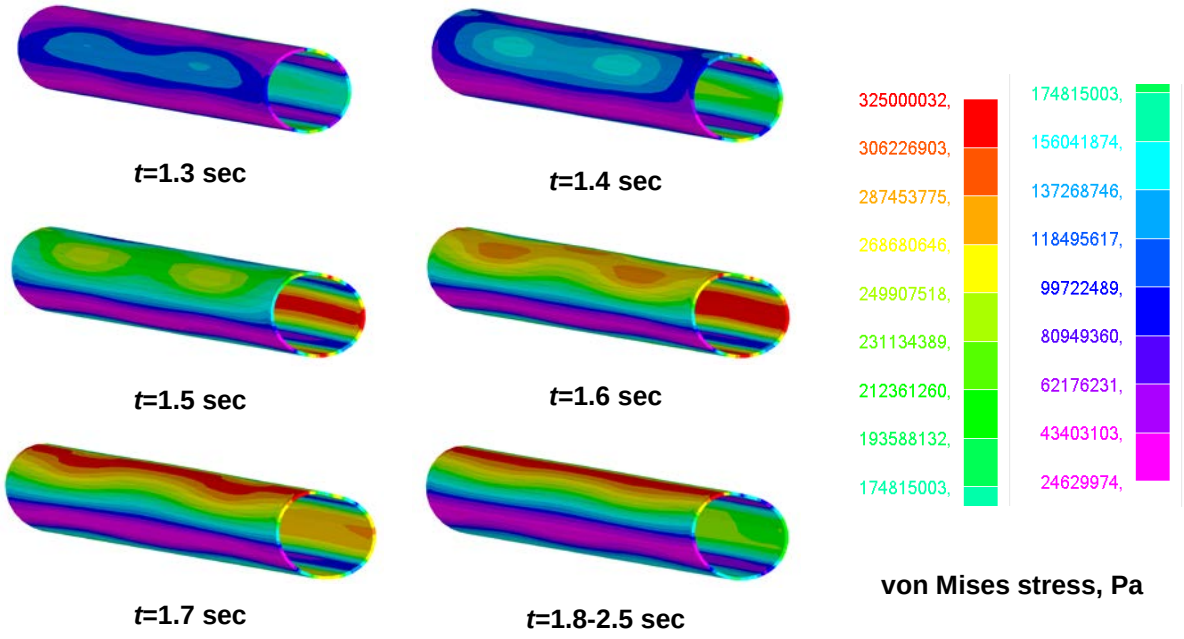

Figure 10. Deformation of the left tubular support during FRCS blast loading.

3.3.2. Asymmetric loading

Calculation of the asymmetric impact showed that with this form of impulse, the load limit value was 26 kPa. This shows an almost equivalent effect in the location of the structure in the immediate spot of the explosion. The nature of the stress redistribution shown in Fig. 11 suggests that the load-carrying capacity margin is higher under this action than under the symmetrical action. Deformation of tubular support is shown in Fig. 12, the limiting value of dynamic load applied to the plate is 39 kPa. It should be noted that the introduction of a damping support here led to a very significant effect, because the limiting load obtained under static loading is 40 kPa. The collapse of the fiber concrete of the structure under this influence begins from the time of 1.3 sec, and by the time of 1.4 sec through formation of cracks is observed, the same as under symmetric loading.

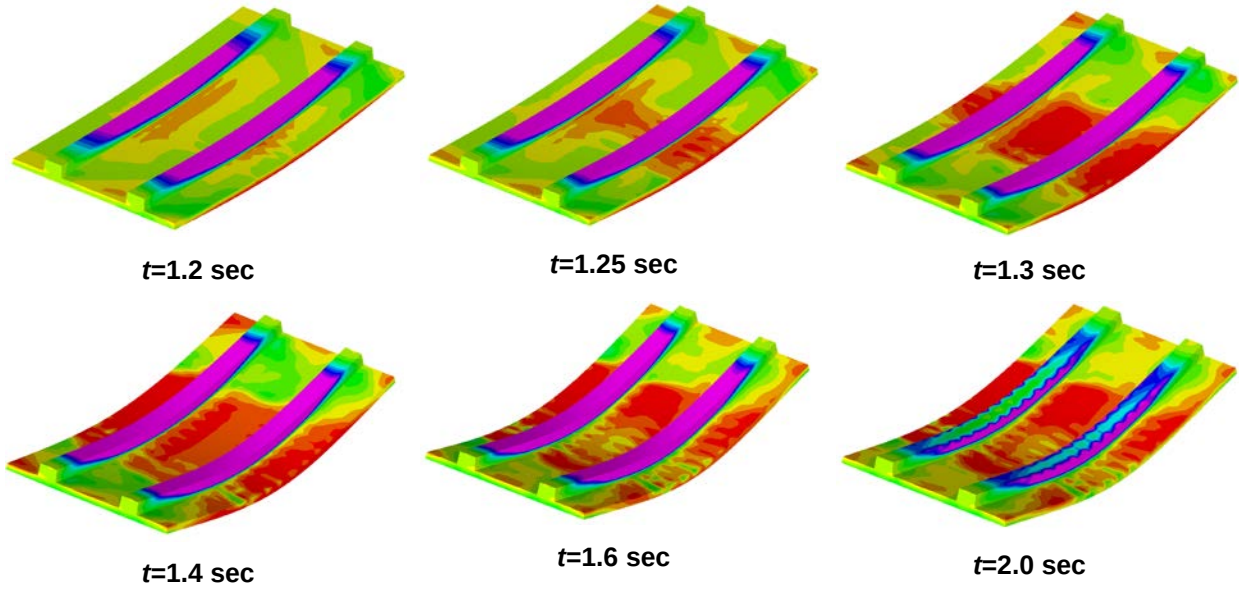

Figure 11. Stress state of fiber concrete under asymmetric loading.

The deformation of the right tubular support here has the character shown in Fig. 12. At a time of 1.4 sec the stress in the upper fiber at the right edge of the steel tube reaches the yield stress, then this stress state is redistributed to the left edge in 0.2 sec and subsequently stress relaxation occurs.

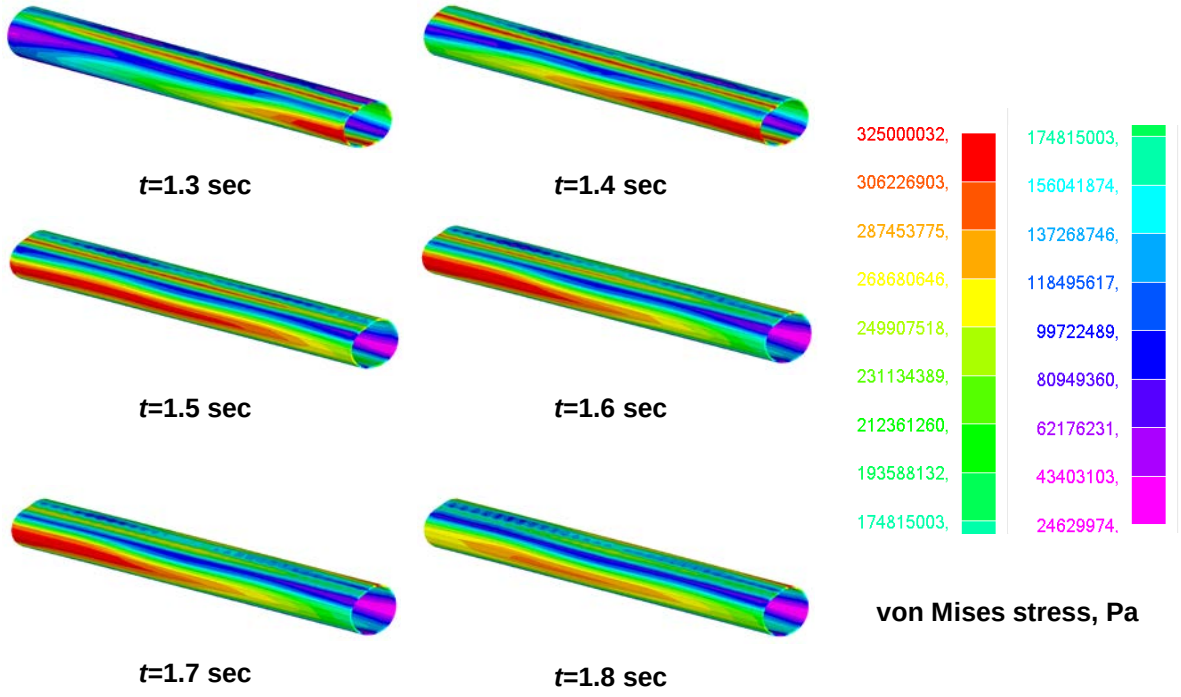

Figure 12. Deformation of the right FRCS tubular support under asymmetric loading.

It is notable that the presence of anchors, providing the connection of the pipe and FRCS, prevents the pipe from detachment and contributes to the dissipation of the blast energy, which is spent on the deformation of the pipe during its loading and unloading. The nature of the contact interaction with the pipe is shown in Figure 13. As can be seen in the figure the stiffness of the tube does not allow for its significant deflections and determines the elastic-plastic nature of the deformations without changing to the rigid body stage. In order to improve the damping properties of the support with the possibility of saving material, a compressible insert inside the pipe is allowed. Comparison of the ultimate load of the obtained calculation results is given in Table 2.

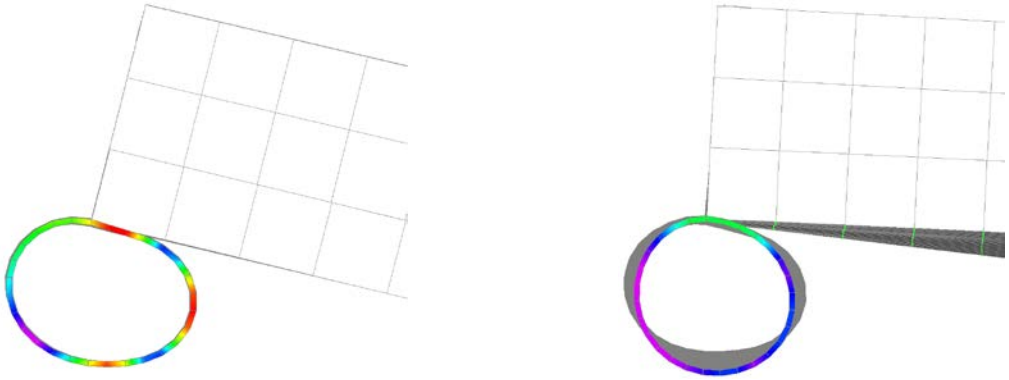

а) **б)**

Figure 13. Deformations of the tubular support considering its contact interaction with FRCS: a) – for symmetric loading; b) – for asymmetric loading.

Table 2. Calculation results of the dynamic load limit value.

Maximum dynamic load				Symmetrical static load (CS2), kPa
symmetrical (CS1), kPa	symmetrical (CS2), kPa	asymmetric (CS1), kPa	asymmetric (CS2), kPa	
25	38	26	39	40
Increasing the intensity dynamic load, %				
–	100(38-25)/25= = **52**	–	100(39-26)/26= = **50**	–

3.4. Discussion

The model of vibration damping is very important in dynamic calculations. In this work, this model is presented on the basis of the combined use of the Rayleigh scheme, which takes into account only the structural damping at the lowest frequencies of the slab vibrations, and the contact finite elements. With the presence of support tubes, damping was considered in the range of 23.1–24.2 Hz, and for rigid supports this interval was 13.7–14.8 Hz. The damping coefficient was assumed to be 0.1, taking into account local structural damage, based on the recommendations of [42]. It is likely that quantitatively different results can be achieved using improved damping models, such as the nonlocal in time model from [41].

The conducted research has prospects both in terms of preparation and conducting of experiments on dynamic effects on buried structures and in terms of selection of rational parameters of reinforcement and stiffnesses of damping supports for structures of this type. The problem of designing rational parameters can be solved using heuristic methods, for example [31], that allow topological synthesis of objects. Thus, as an example, we can consider the possibility of intermittent pipe supports instead of a continuum support.

4. Conclusion

1. The approach to modeling FRCS under dynamic actions with variable in area and intensity loading, simulating blast, taking into account the possible burial of the structure in the ground, including:

- modeling the propagation of dynamic loads using time functions normalized to the value of the peak load;
- an approximate account of the damping of the medium, representing on the one hand the ground and on the other hand the air environment.

2. High efficiency of application of elastoplastic supports for damping vibrations of protective constructions has been revealed. It has been established that the cupping effect in the propagation of progressive destruction of an individual structure can increase the resistance to mechanical damage and the overall level of mechanical safety of structures.

References

1. Quek, J., Chunlin, L., Musngi, J.V., Malalasekara, P.B. A comparison of finite element simulation and experimental results from reinforced concrete columns wrapped with fibre-reinforced polymer subjected to blast loading. 2020. International Journal of Computational Methods and Experimental Measurements. 8 (3). DOI: 10.2495/CMEM-V8-N3-233-242
2. Senthil, K., Gupta, I., Rupali, S., Pelecanos, L. A review on the performance of reinforced concrete structures under blast loading. 2020. Journal of Structural Engineering & Applied Mechanics. 3 (4). DOI: 10.31462/jseam.2020.04216228
3. Isaac, O.S., Jagadeesh, G. Impulse Loading of Plates using a Diverging Shock Tube. 2020. Experimental Mechanics. 60 (4). DOI: 10.1007/s11340-019-00573-5
4. Brekken, K.A., Reyes, A., Børvik, T., Berstad, T., Langseth, M. Sandwich panels with polymeric foam cores exposed to blast loading: An experimental and numerical investigation. 2020. Applied Sciences (Switzerland). 10 (24). DOI: 10.3390/app10249061
5. Li, Y., Chen, Z., Ren, X., Tao, R., Gao, R., Fang, D. Experimental and numerical study on damage mode of RC slabs under combined blast and fragment loading. 2020. International Journal of Impact Engineering. 142. DOI: 10.1016/j.ijimpeng.2020.103579
6. Xu, M., Yang, Y., Lei, H., Wang, P., Li, X., Zhang, Z., Fang, D. Dynamic response of fiber metal laminates subjected to localized high impulse blast loading. 2020. Composite Structures. 243. DOI: 10.1016/j.compstruct.2020.112216
7. Mai, V.C., Vu, N.Q., Nguyen, V.T., Pham, H. Ultra-high performance fiber reinforced concrete panel subjected to severe blast loading. 2020. Defence Science Journal. 70 (6). DOI: 10.14429/DSJ.70.15835
8. Nili, M., Ghorbankhani, A.H., Alavinia, A., Zolfaghari, M. Assessing the impact strength of steel fibre-reinforced concrete under quasi-static and high velocity dynamic impacts. 2016. Construction and Building Materials. 107. Pp. 264–271. DOI: 10.1016/j.conbuildmat.2015.12.161
9. Mishra, N., Netula, O. Behaviour of Reinforced Concrete Framed Structure Subjected to Blast Loading. 2021. International Journal of Advanced Research in Engineering and Technology (IJARET). 12 (1).
10. Mistri, A., Sarkar, P., Davis, R. Column-beam moment capacity ratio and seismic risk of reinforced concrete frame building. 2019. Proceedings of the Institution of Civil Engineers: Structures and Buildings. 172 (3). Pp. 189–196. DOI: 10.1680/jstbu.17.00100
11. Weng, J., Tan, K.H., Lee, C.K. Modeling progressive collapse of 2D reinforced concrete frames subject to column removal scenario. 2017. Engineering Structures. 141. Pp. 126–143. DOI: 10.1016/j.engstruct.2017.03.018
12. Kabantsev, O.V., Tamrazian, A.G. Allowing for changes in the calculated scheme during the analysis of structural behaviour. 2014. Magazine of Civil Engineering. 49 (5). Pp. 15–26 + 123–124. DOI: 10.5862/MCE.49.2
13. Yang, T., Han, Z., Deng, N., Chen, W. Collapse responses of concrete frames reinforced with BFRP bars in middle column removal scenario. 2019. Applied Sciences (Switzerland). 9 (20). DOI: 10.3390/app9204436
14. Kumar, V., Kartik, K.V., Iqbal, M.A. Experimental and numerical investigation of reinforced concrete slabs under blast loading. 2020. Engineering Structures. 206. DOI: 10.1016/j.engstruct.2019.110125
15. Almustafa, M.K., Nehdi, M.L. Machine learning prediction of structural response for FRP retrofitted RC slabs subjected to blast loading. 2021. Engineering Structures. 244. DOI: 10.1016/j.engstruct.2021.112752
16. Chuzel-Marmot, Y., Ortiz, R., Combescure, A. Three dimensional SPH-FEM gluing for simulation of fast impacts on concrete slabs. 2011. Computers and Structures. 89 (23–24). Pp. 2484–2494. DOI: 10.1016/j.compstruc.2011.06.002

17. Del Linz, P., Fan, S.C., Lee, C.K. Modeling of combined impact and blast loading on reinforced concrete slabs. 2016. Latin American Journal of Solids and Structures. 13 (12). Pp. 2266–2282. DOI: 10.1590/1679-78252516
18. Mastali, M., Ghasemi Naghibdehi, M., Naghipour, M., Rabiee, S.M. Experimental assessment of functionally graded reinforced concrete (FGRC) slabs under drop weight and projectile impacts. 2015. Construction and Building Materials. 95. Pp. 296–311. DOI: 10.1016/j.conbuildmat.2015.07.153
19. Zhou, X., Jing, L. Deflection analysis of clamped square sandwich panels with layered-gradient foam cores under blast loading. 2020. Thin-Walled Structures. 157. DOI: 10.1016/j.tws.2020.107141
20. Yang, L., Sui, L., Li, X., Dong, Y., Zi, F., Wu, L. Sandwich plates with gradient lattice cores subjected to air blast loadings. 2021. Mechanics of Advanced Materials and Structures. 28 (13). DOI: 10.1080/15376494.2019.1669092
21. Terrenzi, M., Spacone, E., Camata, G. Collapse limit state definition for seismic assessment of code-conforming RC buildings. 2018. International Journal of Advanced Structural Engineering. 10 (3). Pp. 325–337. DOI: 10.1007/s40091-018-0200-6
22. Lazar Sinković, N., Dolšek, M. Fatality risk and its application to the seismic performance assessment of a building. 2020. Engineering Structures. 205. DOI: 10.1016/j.engstruct.2019.110108
23. Shokrabadi, M., Burton, H.V. Risk-based assessment of aftershock and mainshock-aftershock seismic performance of reinforced concrete frames. 2018. Structural Safety. 73. Pp. 64–74. DOI: 10.1016/j.strusafe.2018.03.003
24. Sinković, N.L., Brozovič, M., Dolšek, M. Risk-based seismic design for collapse safety. 2016. Earthquake Engineering and Structural Dynamics. 45 (9). Pp. 1451–1471. DOI: 10.1002/eqe.2717
25. Thai, D.K., Pham, T.H., Nguyen, D.L. Damage assessment of reinforced concrete columns retrofitted by steel jacket under blast loading. 2020. Structural Design of Tall and Special Buildings. 29 (1). DOI: 10.1002/tal.1676
26. Alekseytsev, A.V. Mechanical safety of reinforced concrete frames under complex emergency actions. 2021. Magazine of Civil Engineering. 103 (3). DOI: 10.34910/MCE.103.6
27. Leppänen, J. Dynamic behaviour of concrete structures subjected to blast and fragment impacts. 2002. … of Structural Engineering, Concrete Structures. …. pp. 96. https://www.msb.se/siteassets/dokument/amnesomraden/krisberedskap-och-civilt-forsvar/befolkningsskydd/skyddsrum/akademiska-avhandlingar/dynamic-behaviour-of-concrete-structures-subjected-to-blast-and-fragment-impacts_lic.pdf
28. Kristoffersen, M., Hauge, K.O., Minoretti, A., Børvik, T. Experimental and numerical studies of tubular concrete structures subjected to blast loading. 2021. Engineering Structures. 233. DOI: 10.1016/j.engstruct.2020.111543
29. Maazoun, A., Matthys, S., Belkassem, B., Atoui, O., Lecompte, D. Experimental study of the bond interaction between CFRP and concrete under blast loading. 2021. Composite Structures. 277. DOI: 10.1016/j.compstruct.2021.114608
30. Li, Z.X., Zhang, X., Shi, Y., Wu, C., Li, J. Finite element modeling of FRP retrofitted RC column against blast loading. 2021. Composite Structures. 263. DOI: 10.1016/j.compstruct.2021.113727
31. Alekseytsev, A.V., Gaile, L., Drukis, P. Optimization of steel beam structures for frame buildings subject to their safety requirements. 2019. Magazine of Civil Engineering. 91 (7). Pp. 3–15. DOI: 10.18720/MCE.91.1
32. Kumpyak, O.G., Galyautdinov, Z.R., Kokorin, D.N. Strength of concrete structures under dynamic loading. AIP Conf. Proc. 2016. 1698. 070006. DOI: 10.1063/1.4937876
33. Nguyen, W., Bandelt, M.J., Trono, W., Billington, S.L., Ostertag, C.P. Mechanics and failure characteristics of hybrid fiber-reinforced concrete (HyFRC) composites with longitudinal steel reinforcement. 2019. Engineering Structures. 183. Pp. 243–254. DOI: 10.1016/j.engstruct.2018.12.087
34. Kyriakides, N., Sohaib, A., Pilakoutas, K., Neocleous, K., Chrysostomou, C., Tantele, E., Votsis, R. Evaluation of Seismic Demand for Substandard Reinforced Concrete Structures. 2018. The Open Construction and Building Technology Journal. 12 (1). Pp. 9–33. DOI: 10.2174/1874836801812010009
35. An, H., Hou, S., Liu, L. Experimental and numerical study of the concrete stress and fracture propagation processes by blast. 2019. Engineering Letters. 27 (4). Pp. 1–7.
36. Chen, Y., May, I.M. Reinforced concrete members under drop-weight impacts. 2009. Proceedings of the Institution of Civil Engineers: Structures and Buildings. 162 (1). Pp. 45–56. DOI: 10.1680/stbu.2009.162.1.45
37. Qasrawi, Y., Heffernan, P.J., Fam, A. Dynamic behaviour of concrete filled FRP tubes subjected to impact loading. 2015. Engineering Structures. 100. Pp. 212–225. DOI: 10.1016/j.engstruct.2015.06.012
38. Ngo, T., Mendis, P. Modelling the dynamic response and failure modes of reinforced concrete structures subjected to blast and impact loading. 2009. Structural Engineering and Mechanics. 32 (2). Pp. 269–282. DOI: 10.12989/sem.2009.32.2.269
39. Niroomandi, A., Pampanin, S., Dhakal, R.P., Ashtiani, M.S., De La Torre, C. Rectangular RC walls under bi-directional loading: recent experimental and numerical findings. Hamilton: 2018 New Zealand Concrete Industry Conference. 11/10/2018-13/10/2018
40. Magnusson, J., Hallgren, M., Ansell, A. Shear in concrete structures subjected to dynamic loads. 2014. Structural Concrete. 15 (1). Pp. 55–65. DOI: 10.1002/suco.201300040
41. Sidorov, V., Badina, E., Detina, E. Nonlocal in time model of material damping in composite structural elements dynamic analysis. 2021. International Journal for Computational Civil and Structural Engineering. 17 (4). Pp. 14–21. DOI: 10.22337/2587-9618-2021-17-4-14-21
42. Russell, J.M., Owen, J.S., Hajirasouliha, I. Experimental investigation on the dynamic response of RC flat slabs after a sudden column loss. 2015. Engineering Structures. 99. DOI: 10.1016/j.engstruct.2015.04.040
43. Mkrtychev, O., Savenkov, A. Modeling of blast effects on underground structure. 2019. International Journal for Computational Civil and Structural Engineering. 15 (4). DOI: 10.22337/2587-9618-2019-15-4-111-122
44. Giam, A., Toh, W., Tan, V.B.C. Numerical review of Jones-Wilkins-Lee parameters for trinitrotoluene explosive in free-air blast. 2020. Journal of Applied Mechanics, Transactions ASME. 87 (5). DOI: 10.1115/1.4046243
45. Garno, J., Ouellet, F., Bae, S., Jackson, T.L., Kim, N.H., Haftka, R., Hughes, K.T., Balachandar, S. Calibration of reactive burn and Jones-Wilkins-Lee parameters for simulations of a detonation-driven flow experiment with uncertainty quantification. 2020. Physical Review Fluids. 5 (12). DOI: 10.1103/PhysRevFluids.5.123201
46. Castedo, R., Natale, M., López, L.M., Sanchidrián, J.A., Santos, A.P., Navarro, J., Segarra, P. Estimation of Jones-Wilkins-Lee parameters of emulsion explosives using cylinder tests and their numerical validation. 2018. International Journal of Rock Mechanics and Mining Sciences. 112. DOI: 10.1016/j.ijrmms.2018.10.027

Information about authors:

Anatoly Alekseytsev, *Doctor of Technical Science*
ORCID: https://orcid.org/0000-0002-4765-5819
E-mail: aalexw@mail.ru

Svetlana Sazonova,
ORCID: https://orcid.org/0000-0003-4025-2053
E-mail: s.sazonovaa17@mail.ru

Received 06.05.2022. Approved after reviewing 28.09.2022. Accepted 06.10.2022.